7392 *Biochemistry* **2009,** *48,* 7392–7398
DOI: 10.1021/bi9006836

BIOCHEMISTRY
including biophysical chemistry & molecular biology
Article

Novel Molecular Mechanism for Actinomycin D Activity as an Oncogenic Promoter G-Quadruplex Binder†

Hyun-Jin Kang and Hyun-Ju Park*

College of Pharmacy, Sungkyunkwan University, Suwon 440-746, Republic of Korea

Received April 21, 2009; Revised Manuscript Received May 20, 2009

ABSTRACT: Actinomycin D (ActD) is a natural antibiotic that inhibits the transcription of genes by interacting with a GC-rich duplex, a single-stranded or hairpin form of DNA, and then interfering with the action of RNA polymerase. In this study, we identified a novel molecular mechanism of anticancer activity of ActD as an oncogenic c-Myc promoter G-quadruplex binder. ActD selectively inhibits the elongation of oligonucleotides containing c-Myc promoter G-quadruplex sequence in PCR-stop assays. UV−vis spectroscopic and circular dichroism studies suggest that ActD interacts with c-Myc promoter G-quadruplex via a surface end stacking interaction, inducing a mixed-type conformation of the G-quadruplex. ActD selectively inhibits the cellular growth and synthesis of c-Myc mRNA in Ramos cells having the $NHEIII_1$ region in the translocated c-Myc gene. In addition, the results of promoter assays using two kinds of $NHEIII_1$ region mutants and wild-type constructs strongly support the idea that binding of ActD with G-quadruplex formed in the promoter region results in the reporter gene being turned off. Our study reveals a novel mechanism underlying the anticancer activity of ActD, whereby ActD interacts with oncogenic promoter G-quadruplex DNA to repress gene expression.

The G-quadruplex is noncanonical secondary structure of nucleic acid with a G-rich sequence and forms Hoogsteen base pairings (*1*) (Figure 1a). It is well-known that the G-rich telomere may be folded into G-quadruplex and inhibits the telomere elongation by telomerase due to a structural obstacle (*2*). G-Rich repeats have also been found in the promoter regions of cell proliferation-related genes (*3*) and appear to be a *cis* regulator of gene transcription. Actually, several oncogenes, such as c-*myc* (*4*, *5*), c-*kit* (*6*), KRAS (*7*), and Bcl2[1] (*8*), and metastasis-related genes, such as VEGF (*9*) and HIF-1α (*10*), are controlled by G-quadruplex formed in their promoter regions. Therefore, the developments of oncogenic G-quadruplex binding ligands and telomere G-quadruplex are novel therapeutic approaches to cancer treatment (*11*−*13*).

Several DNA binding ligands with antibiotic effects, such as berberine, distamycin, and quercetin, exhibited G-quadruplex binding activities (*14*−*16*), which implies that their biological effects are related to binding with this novel secondary DNA structure. Actinomycin D (ActD) is a natural antibiotic (Figure 1b) that inhibits the transcriptions of genes and then represses the proliferation of cancer cells (*17*). In addition to its classical binding with GC-rich DNA, ActD has been reported to have binding activity for nonduplex DNA, such as single-stranded (*18*−*23*) or hairpin (*24*, *25*) structures. Another study showed that the intermolecular G-quadruplex formed in the presence of low concentrations of ammonium is disintegrated by ActD (*26*), and recently, biophysical analysis revealed that ActD binds to the telomeric G-quadruplex (*27*, *28*), which implies a direct interaction between ActD and G-quadruplex.

c-Myc is one of the best known oncogenes, and it is over-expressed in various cancer cells, playing a role as a transcriptional factor that regulates the cell cycle, cellular proliferation, and apoptosis (*29*, *30*). Oncogenic c-Myc is mainly regulated by nuclease hypersensitivity element III_1 ($NHEIII_1$) located between nucleotides −115 and −142 upstream of the P1 promoter, which controls 80−90% of the transcription level of c-Myc (*31*, *32*). This $NHEIII_1$ region contains 27 guanine-rich bases in its antisense strand (Figure 1c), which can be folded into G-quadruplex that plays a role as a transcription repressor (*4*, *5*). Vaquero and Portugal found that ActD inhibited the transcription of c-Myc by binding to its promoter region within the sequence of nucleotides −110 to 68 from the P1 promoter at 0.5 and 5 μM, and interrupting the interaction between the Sp1 transcription factor and promoter in vitro (*33*). In this study, we identified that G-quadruplex structure formed in the $NHEIII_1$ region, upstream of the above-described site, should be a target for ActD, and we subsequently examined the biological consequences of their interaction. Our study suggests a new molecular mechanism for the anticancer effect of ActD, which

†This work was supported by a Korea Science and Engineering Foundation (KOSEF) grant funded by the Korea government (MEST) (R01-2008-000-20771-0).

*To whom correspondence should be addressed: College of Pharmacy, Sungkyunkwan University, Suwon 440-746, Republic of Korea. Phone: +82-31-290-7719. Fax: +82-31-292-8800. E-mail: hyunju85@skku.edu.

[1]Abbreviations: ActD, actinomycin D; $NHEIII_1$, nuclease hypersensitive element III_1; WT, wild-type; MF, major form; Mut, mutant; Bcl2, B-cell CLL/lymphoma 2; VEGF, vascular endothelial growth factor; HIF-1α, hypoxia-inducible factor-1; PAGE, polyacrylamide gel electrophoresis.

 Published on Web 06/04/2009

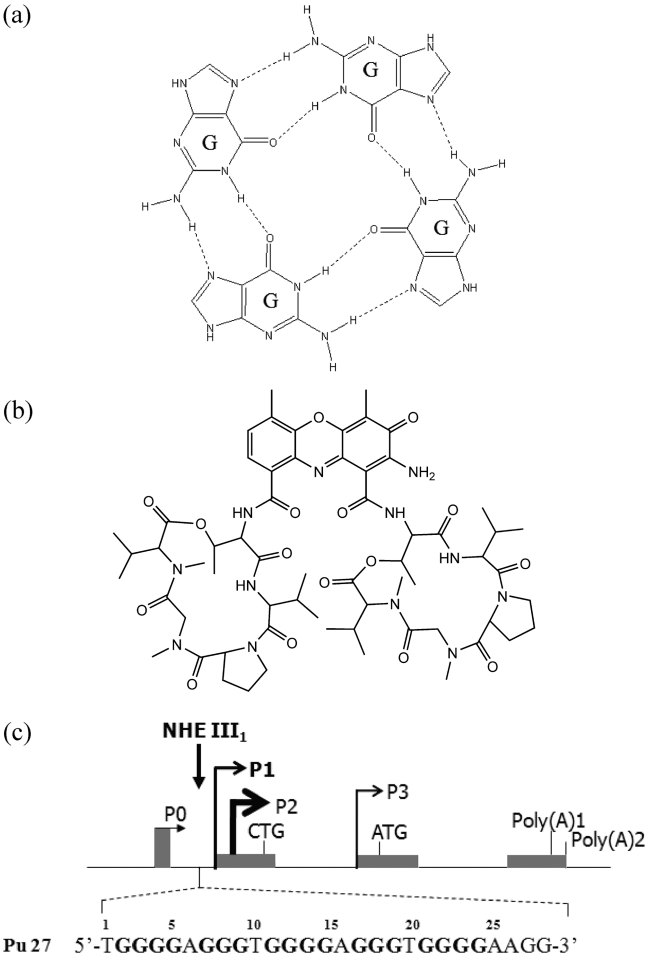

FIGURE 1: (a) Hoogsteen base pairing in G-quadruplex. (b) Structure of actinomycin D (ActD). (c) Nuclease hypersensitivity element ($NHEIII_1$) region of the c-Myc P1 promoter. The Pu27 sequence is displayed with numbers.

involves binding of ActD to oncogenic promoter G-quadruplex and the subsequent inhibition of c-Myc transcription.

MATERIALS AND METHODS

PCR-Stop Assays. Oligonucleotides for PCR-stop assays were synthesized by Bionics or Bioneer Co. (Seoul) and purified via 6 M urea-denatured PAGE. Sequences of oligonucleotides for the PCR-stop assay are listed in Table S1 of the Supporting Information. Actinomycin D (Sigma-Aldrich, catalog no. A1410) was dissolved in DMSO. Taq polymerase and dNTP mixtures were purchased from Koma Biotech. PCR-stop assays (*34*) were performed in a reaction buffer containing 10 mM Tris-HCl (pH 8.3), 50 mM KCl, and 1.5 mM $Mg(OAc)_2$ with each oligonucleotide at 0.2 μM. Polymerase chain reaction (PCR) cycling involved an initial denaturation at 94 °C for 2 min, followed by 30 cycles of 94 °C for 30 s, 58 °C for 30 s, and 72 °C for 30 s. PCR products were purified by 15% native PAGE (1× TBE) and stained with SYBR Green I (Roche). The fluorescence intensity of the PCR product bands was read using a FLA-2000 unit and analyzed using Multigauge (Fujifilm).

UV−Vis Spectroscopy and CD. Oligonucleotide Pu27 for UV−vis and CD spectroscopy studies was synthesized by Bioneer (Seoul, Korea) and HPLC-purified. Pu27 for UV−vis spectroscopy and CD studies was heated at 95 °C for 10 min in buffer and then slowly cooled to room temperature overnight.

UV−vis absorbance spectra were recorded using a Shimadzu 1600 personal computer. Concentrations of DNA and ActD were determined in buffer containing 10 mM Tris-HCl (pH 7.6) and 100 mM KCl using the Beer−Lambert law based on the absorbance at 260 nm and a molecular extinction coefficient [$\varepsilon = 2.153 \times 10^5$ M^{-1} cm^{-1} (*35*)] for Pu27 and the absorbance at 440 nm and an ε of 24800 M^{-1} cm^{-1} (*36*) for ActD. The absorbance spectrum of 10 μM ActD in 200 μL of buffer was recorded, and this was followed by incrementally adding annealed intramolecular 100 μM Pu27 (*37*). Raw data were corrected for dilution using the relationship $A_{corr} = A_{exp} \times (200+V)/200$, where V is the volume of the added DNA solution (*38*). For continuous variation analysis (Job plot), both ActD and the annealed Pu27 were diluted to a final concentration of 10 μM with buffer. Solutions of ActD and Pu27 were produced at various volume ratios of ActD to Pu27 (from 0.15 to 0.95) while the total volume was kept at 200 μL.

CD spectra were recorded using a Jasco-810 spectropolarimeter (Jasco, Easton, MD) using a quartz cell with an optical path length of 1 mm in the wavelength range of 210−500 nm at 20 °C; the bandwidth was 0.5 nm, the scanning speed 100 nm/min, and the response time 1 s. Pu27 (5 μM) was annealed in a buffer containing 10 mM Tris-HCl (pH 7.4) and 5 mM KCl overnight with 0.1% DMSO as a control or with ActD. A low potassium ion concentration is used considering exceptional stability of Pu27. To measure thermal stabilities, the temperature was increased from 20 to 90 °C at a rate of 0.5 °C/min and ellipticity at 262 nm was recorded using a 0.5 nm bandwidth. Melting curves were normalized using the expression $(E_{temperature} - E_f)/(E_{98°C} - E_f)$, where $E_{temperature}$ is the ellipticity read at each temperature and E_f is the maximum ellipticity of the folded state.

Cytotoxicity Assays. To study the cytotoxic effect of ActD, Ramos and CA46 cell lines were treated with different concentrations of ActD. The Ramos cell line was obtained from the Korean Cell line bank (KCLB, catalog no. 21596) and the CA46 cell line from ATCC (catalog no. CRL 1648). Both cell lines were cultured in RPMI-1640 containing 10% FBS and 1% penicillin/streptomycin (purchased from Hyclone). After cells had been treated with ActD for 24 h, cell proliferation assays were performed using MTS reagent (Promega, catalog no. G3580). The same volume of DMSO was treated for a control.

Real-Time PCR. Total RNA was isolated from Ramos and CA46 cells cultured in 12-well plates with treatment of ActD for 24 h using Easy-Blue RNA extraction kits (Intron Biotechnology). Concentrations of total RNA were determined by the absorbance at 260 nm, and cDNA synthesis was performed using Maxime RT PreMix kits (Intron Biotechnology).

Real-time PCR was performed using Master Mixture containing SYBR Green I (Kapa SYBR FAST qPCR Kit) and a *Line-gene K* real-time PCR detection system (Bioer Technology). PCR was performed using an initial denaturing at 95 °C for 3 min, followed by 40 cycles of 95 °C for 15 s and 60 °C for 45 s. Melting curves was obtained using 0.5 °C steps and an incubation time of 30 s. The following primers were used in this study: 5′-TCAAGAGGCGAACACACAAC-3′ (forward) and 5′-GGCCTTTTCATTG-TTTTCCA-3′ (reverse) for c-Myc (*39*) and 5′-GGACTTCGAGCAAGAGATGG-3′ (forward) and 5′-AGCACTGTGTTGGCGTACAG-3′ (reverse) for β-actin (*40*).

Promoter Assay. Three types of pGL3 constructs were used. pGL3-Pu27 had the wild-type $NHEIII_1$ region of c-Myc upstream of the firefly luciferase gene; pGL3-ΔPu27 did not have

Table 1: Sequences and IC_{50} Values of ActD for the PCR-Arresting Effect against Several Oncogenic G-Quadruplex-Forming Oligonucleotides[a]

name	sequence	IC_{50} (μM)
c-myc Pu26WT	TGGGGAGGGTGGGGAGGGTGGGGAAG	2.7 ± 0.19
c-myc Pu26MF	TGGGGAGGGTGGGTAGGGTGGGTAAG	2.2 ± 0.1
c-myc Pu26Mut	TGGGGAGGGTGAGGAGGGTGGGGAAG	69.7 ± 11.5
Bcl2	AGGGGCGGGCGCGGGAGGAAGGGGGCGGGAGCGGGGCTG	10.4 ± 0.7
HIF-1α	GCGGGGAGGGGAGAGGGGGCGGGAGC	12.7 ± 0.65
VEGF	TAGGGGCGGGCCGGGGGCGGGGAGC	9.8 ± 0.60

[a] WT, MF, and Mut denote wild-type, major form, and mutant, respectively.

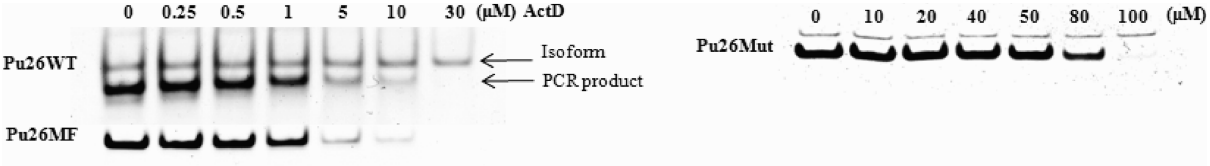

FIGURE 2: Concentration-dependent PCR-arresting effects of ActD against Pu26WT, Pu26MF, and Pu26Mut. ActD had a selective PCR-arresting effect on the G-quadruplex-forming oligonucleotides in the c-Myc promoter. The PCR product of 38 bp was isolated by 15% native PAGE, stained with SYBR Green I, and analyzed using Multi-Gauge (Fujifilm). MF and Mut denote major form and mutant, respectively.

this region, and pGL3-Mut had a one-point mutated sequence in this region. The scheme used for cloning these constructs is shown in Figure S1 of the Supporting Information. HeLa cells (4×10^4) were precultured in Dulbecco's modified Eagle's medium (DMEM) containing 10% fetal bovine serum and 1% penicillin/streptomycin (Hyclone) for 24 h. Cells were transfected with pGL3 constructs using WelFect transfection kits (Welgene), following the manufacturer's instructions. For normalization of transfection efficiency, 25 ng of pRL-TK was cotransfected. ActD was treated for 24 h, and cells were harvested by scraping in PBS buffer and cell pellets lysed using passive lysis buffer (Promega). The supernatant of cell lysate was used to perform dual-luciferase assays (Promega) using a 20/20n single tube luminometer (Turner Biosystems).

Molecular Modeling. A complex structure of ActD and mixed parallel- and antiparallel-stranded c-Myc quadruplex was manually constructed on the basis of the NMR structure (Protein Data Bank entry 2A5R). Manual replacement of TMPyP4 with ActD and the location of two potassium ions between the three G-stacks were conducted using the Biopolymer module in SYBYL version 7.3 (Tripos Inc., St. Louis, MO). This structure was optimized in the explicit system by using the SANDER module in AMBER 8.0 (http://ambermd.org). Parameters for ActD were generated using the Antechamber module. Parameters such as the atom radius and the charge of potassium ion were assigned with the Xleap module. To prepare for the running of the SANDER module, the molecule was surrounded by a truncated octahedral TIP3P water box with a 10 Å water layer and neutralized by potassium ions. Prior to the molecular dynamics calculation, steepest descent minimizations with two steps were performed to equilibrate the water boxes and ions and to remove improper interactions between molecules. Molecular dynamics calculations were performed using periodic boundaries and the shake algorithm in two steps. The first step involved fixing the positions of the molecules to equilibrate the added water boxes with DNA and second step for the whole system for 2 ns. The temperature during molecular dynamics was kept at 300 K and was controlled using the Langevin algorithm under 1 atm of pressure. To analyze MD results, a DNA backbone root-mean-square deviation (rmsd) calculation was performed using the ptraj module in AMBER. Trajectories with a constant rmsd were averaged using the ptraj module, and the structure was finally minimized using the explicit system.

RESULTS AND DISCUSSION

PCR-Stop Assay. To identify the binding potency of ActD with the $NHEIII_1$ region of the c-Myc promoter, PCR-stop assays were performed using various types of oligonucleotides modified from Pu27 (Figure 1c) as templates and primers for PCR; Pu27 is the oligonucleotide with the same sequence as $NHEIII_1$. As listed in Table 1, Pu26WT is made by deleting the 3′-end guanine residue of Pu27, Pu26MF is a dual G14T/G23T mutant, and Pu26Mut is a single G12A mutant. Pu26WT and Pu26MF are known to form stable intramolecular G-quadruplex (*41*), while Pu26Mut could not do so.

ActD had a similar PCR-arresting effect on Pu26WT and Pu26MF, with ~25-fold selectivity over Pu26Mut (Figure 2). The results indicate that ActD interacts with the intramolecular G-quadruplex derived from Pu26WT and Pu26MF and may stabilize the G-quadruplex structure. PCR-stop assays using the other oncogenic G-quadruplex-forming oligonucleotides of Bcl-2, VEGF, and HIF-1α showed that ActD bound to them with rather lower activity than c-Myc (Pu26WT), as summarized in Table 1. In the case of Bcl-2, it has already been reported that its expression is downregulated by ActD (*42*). Our result suggests that a direct interaction between ActD and the promoter G-quadruplex of Bcl-2 is related to transcriptional repression.

Spectroscopic Studies on the Interaction between ActD and Pu27. To investigate the direct interaction between ActD and c-Myc promoter G-quadruplex, the UV−visible absorbance spectrum of ActD was recorded at different DNA concentrations. ActD exhibited 48 ± 2% hypochromicity without a bathochromic shift, illustrated in Figure 3a. This phenomenon suggests that the environment around a chromophore is unchanged after binding with DNA bases (*43*), implying that ActD causes a stacking interaction between the phenoxazone ring and any guanine at the end surface of the G-quartet.

Continuous variation binding analysis showed evidence of two binding stoichiometries of ActD with Pu27. As shown in

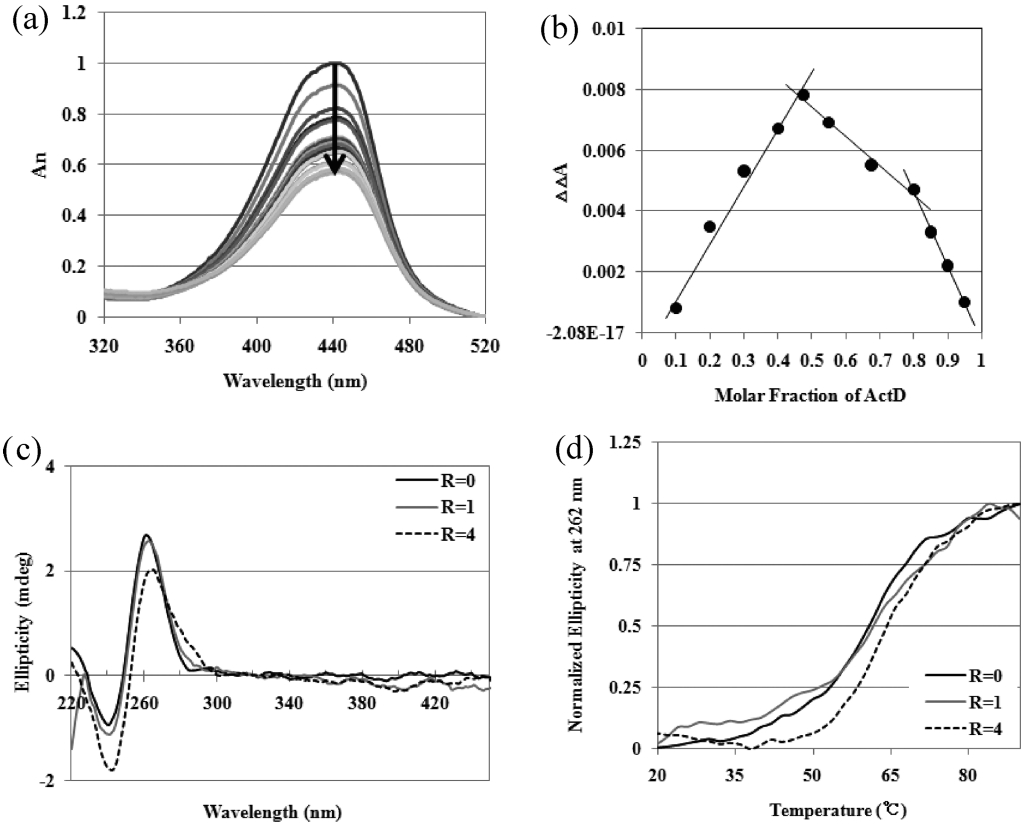

FIGURE 3: Spectroscopic analysis. (a and b) UV−vis spectroscopic analysis in 10 mM Tris-HCl (pH 7.6) and 100 mM KCl. (a) Changes in the absorbance spectrum of ActD with respect to Pu27. The arrow represents spectral changes of 10 μM ActD caused by an increasing concentration of Pu27. A_n is the normalized absorbance (A/A_{443}). (b) Continuous variation binding analysis (Job plot) of ActD. The total concentration of ActD and Pu27 was kept at 10 μM. As a control, only buffer, instead of Pu27, was added to ActD. The absorbance difference between 425 and 475 nm of ActD in buffer and Pu27 was determined, and the difference (ΔA) between buffer and Pu27 was used to plot. $\Delta\Delta A = A_{bfr(A_{425} - A_{475})} - A_{Pu27(A_{425} - A_{475})}$. (c and d) CD spectrum and melting curve in 10 mM Tris-HCl (pH 7.4) and 5 mM KCl. (c) Effect of ActD on the conformational changes of Pu27. ActD induced various conformations of Pu27 depending on the binding ratio. The spectrum of buffer with DMSO or ActD was subtracted from spectra of samples with Pu27 in buffer. (d) Melting curves of Pu27 and ActD complex. The spectral change at 262 nm was monitored while the temperature was increased at a rate of 0.5 °C/min. R = [ActD]/[Pu27].

Figure 3b, the first intersection point was at 0.48 ± 0.01 and the second at 0.79 ± 0.02, indicating approximately 1:1 and 4:1 (ActD:Pu27) molar binding ratios, respectively. In the case of TMPyP4, a well-known G-quadruplex binder, it also interacts with the c-Myc quadruplex by various stoichiometries, including 1:1 and 1:4 (*35*).

The effect of ActD on the conformational change of Pu27 was examined by CD analysis. The maximum ellipticity of Pu27 at 262 nm and the minimum ellipticity at 240 nm are the signatures of parallel-stranded G-quadruplexes (*44*). To minimize the effect of potassium ion, a strong G-quadruplex stabilizing cation, on the stability of G-quadruplex, a low concentration of K^+ was used. In 5 mM KCl buffer, 1:1 and 1:4 Pu27:ActD complex ratios induced a shoulder at ~290 nm (Figure 3c), which means mixed parallel/antiparallel strand of c-Myc quadruplex (*45*). Melting curves of Pu27 and ActD with respect to two binding ratios revealed no significant change in T_m for a 1:1 mixture and a small increase for a 1:4 mixture (Figure 3d). In the case of interaction between ActD and telomeric G-quadruplex d[AGGG-(TTAGGG)$_3$] (*28*), mixed parallel/antiparallel conformation of DNA was also induced in K^+ buffer. Via binding of ActD with a 1:2 ratio (ActD:G-quadruplex) via surface end stacking, telomeric G-quadruplex exhibited a large conformational change and increased ΔT_m. Remarkable changes in conformation and ΔT_m could not be observed in Pu27 complexed with ActD unlike telomeric G-quadruplex, since Pu27 has short single-nucleotide loops which provide a higher stability of G-quadruplex structure (*46*). However, it does not necessarily mean the weak binding of ActD with c-Myc quadruplex, considering the low correlation between binding constant (K_d) and melting temperature (T_m) of G-quadruplex binding ligands reported previously (*47*).

Hurley suggested that binding of a small ligand to the G-quadruplex changes the molecular recognition property of the G-quadruplex and subsequent molecular signaling (*13*). In contrast to known G-quadruplex binders that stabilize c-Myc quadruplex structure functioning as transcription repressors, polyamines (spermidine and spermine) were reported to bind to c-Myc quadruplex and produce a structural switch from the c-Myc quadruplex to a transcriptionally active form (*48*). Taken together, it is possible that ActD may induce the mixed-type stranded conformation of G-quadruplex with transcription repressing activity reminiscent of that caused by Se2SAP (*49*).

We built a model of ActD stacked at the end surface of c-Myc promoter G-quadruplex. Analysis of molecular dynamics revealed that the calculated potential energy of the mixed-type G-quadruplex and ActD complex (Figure S2 of the Supporting Information) is lower than that of the parallel-stranded G-quadruplex and ActD complex in spite of the absence of any hydrogen bonding interaction between the two molecules (Figure 4a). As shown in Figure 4b, the methyl group attached to the phenoxazone ring and aliphatic groups of the side chains in the two cyclic peptides of ActD are located close to the nonpolar

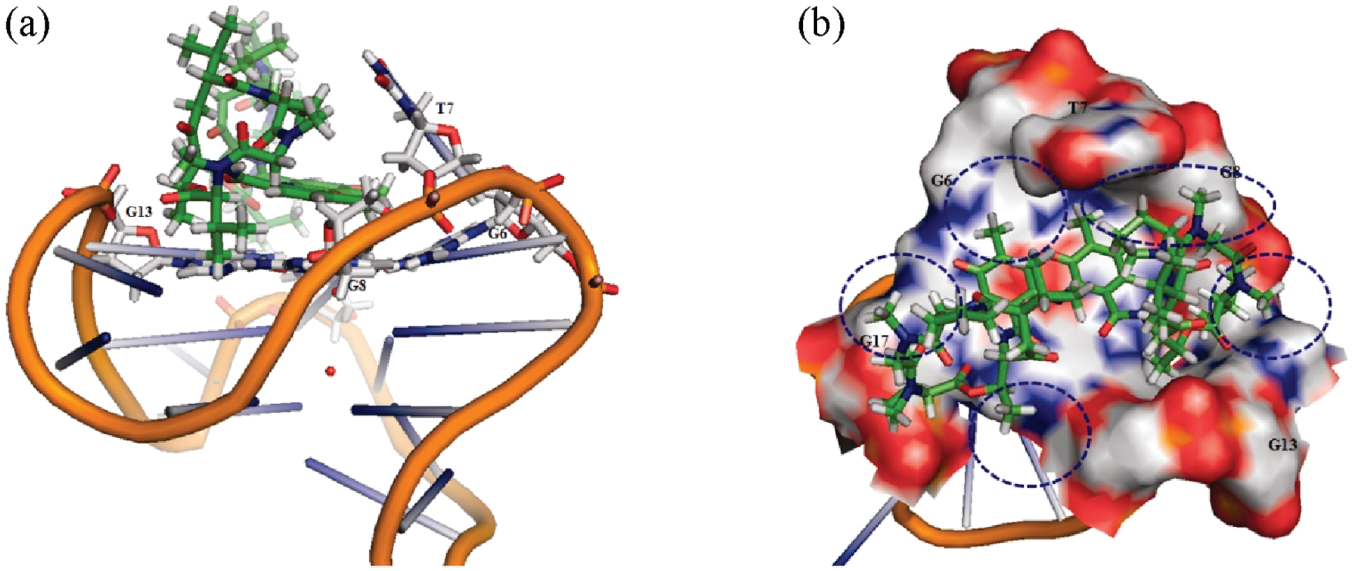

FIGURE 4: Molecular model of mixed parallel- and antiparallel-stranded Pu27 and ActD complex structure. ActD is colored green and Pu27 white. Molecular dynamics of the structure were determined in an octahedral water box for 2 ns at 300 K. (a) Front view of the complex structure. The two red-colored spheres are potassium ions, and several sticks represent bases. The orange-colored tubes represent DNA backbones. (b) From the top view of the complex structure, the van der Waals interactions between ActD and Pu27 are shown by blue-dotted circles. These models were produced using PyMol (http://pymol.sourceforge.net).

portion (white-colored) of bases and sugars of DNA, suggesting that ActD interacts with G-quadruplex mainly by van der Waals or hydrophobic forces.

Cell-Based Study of ActD Targeting the NHEIII$_1$ Region of c-Myc. Although ActD is a nonspecific transcription inhibitor, low concentrations of ActD were found to selectively inhibit the transcription of proto-oncogenes, such as c-*myc*, c-*fos*, and c-*jun* (*50*). Therefore, a low concentration of ActD was used against cells in the cell-based studies. In Ramos and CA46 cell lines (both Burkitt's lymphoma cell lines), c-Myc on chromosome 8 is translocated into the Ig switch region on chromosome 14, and the transcription of translocated c-Myc is regulated by different promoters (*51*). The upstream promoter region, including NHEIII$_1$, is cotranslocated with the c-Myc gene into the Ig switch region in the Ramos cell line, which controls the overexpression of the c-Myc gene, whereas this element is not present in the CA46 cell line (*4*).

The cytotoxic effect of ActD against two Burkitt's lymphoma cells was examined using proliferation assays using MTS reagent. ActD more sensitively inhibited the proliferation of Ramos cells than CA46 cells (Figure S3 of the Supporting Information). The effects of ActD on c-Myc mRNA synthesis in these cell lines were compared by real-time PCR (Figure 5a). ActD lowered the level of c-Myc mRNA more effectively in Ramos cells than in CA46 cells in a concentration-dependent manner. The results demonstrate that ActD interacted selectively with G-quadruplex in the NHEIII$_1$ region of the c-Myc promoter and inhibited transcription, which may result in higher cytotoxicity.

To confirm the effect of ActD on transcriptional changes of the c-Myc gene due to interaction with Pu27 in NHEIII$_1$, a promoter assay was performed. Three types of plasmids were constructed and transfected into HeLa cells. Pu27 had a wild-type sequence in the NHEIII$_1$ region; ΔPu27 is a deletion mutant without ~100 bp, which included the NHEIII$_1$ region, and Mut is the point mutant, which cannot fold into stable intramolecular G-quadruplex structure (the same as Pu26Mut used in the PCR-stop assay). As a result, ActD was found to selectively

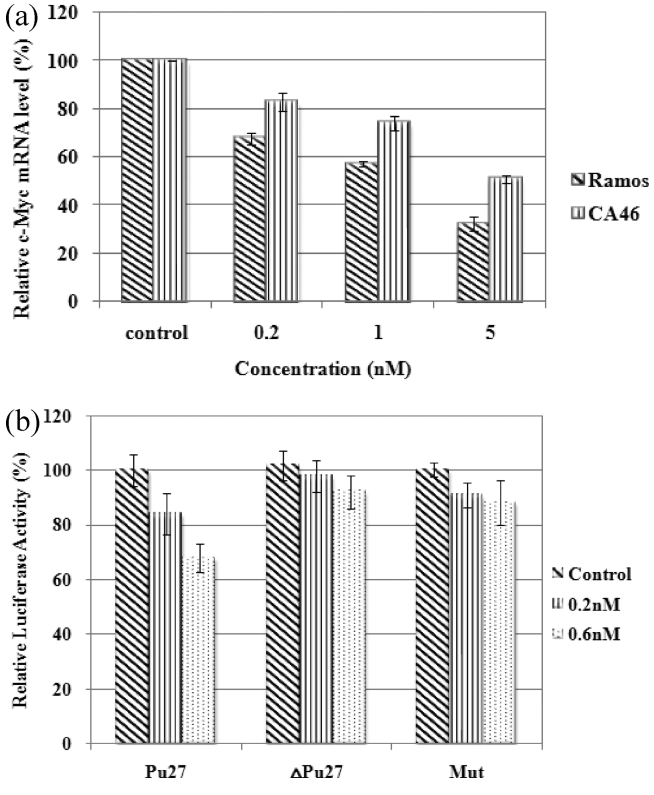

FIGURE 5: Different biological effects of ActD against two Burkitt's lymphomas. (a) Different effects of ActD on c-Myc mRNA synthesis in two different Burkitt's lymphoma cell lines. Several concentrations of ActD were employed for 24 h. ActD exhibited more sensitive inhibition of mRNA synthesis in Ramos than CA46 cells. Real-time PCR was performed using SYBR Green I to detect PCR products. The same volume of DMSO was added to the control wells. β-Actin was used as the internal standard. Three independent experiments were performed. (b) Result of the promoter assay. The three construct types were transfected for 6 h, and drugs were then administered for 24 h. ActD selectively decreased the level of expression of firefly luciferase transcribed from wild-type Pu27. pRL-TK was cotransfected to normalize for transfection efficiency. The same volume of DMSO was treated as a control.

inhibit the luciferase expression of the Pu27 construct (Figure 5b). Treatment with 1 nM ActD resulted in the non-specific inhibition of luciferase expression for all construct types (data not shown). These results imply that ActD at low concentrations selectively interacts with the G-quadruplex structure formed in the $NHEIII_1$ region and then turns off gene expression.

CONCLUSIONS

Through this study, a novel molecular mechanism of c-Myc transcription inhibition by ActD was investigated, and ActD was identified as a c-Myc promoter G-quadruplex binder. Biophysical analyses revealed that ActD produced a sequence-specific PCR arresting effect by directly interacting with intramolecular G-quadruplex in c-Myc promoter. In cell-based studies, ActD was found to repress c-Myc mRNA synthesis selectively in Ramos cells, which overexpress c-Myc promoted by the $NHEIII_1$ region containing G-quadruplex-forming sequences. On the basis of the results from this study, we are working on the development of phenoxazone derivatives which may interact selectively with the oncogenic promoter G-quadruplex and give excellent anticancer activity.

SUPPORTING INFORMATION AVAILABLE

Sequences of primers used in the PCR-stop assay, cloning constructs for the promoter assay, calculated potential energies of G-quadruplex−actinomycin D complexes, and cytotoxicity of actinomycin D against Ramos and CA46 cells. This material is available free of charge via the Internet at http://pubs.acs.org.

REFERENCES

(1) Ghosal, G., and Muniyappa, K. (2006) Hoogsteen base-pairing revisited: Resolving a role in normal biological processes and human diseases. *Biochem. Biophys. Res. Commun. 343*, 1–7.

(2) Neidle, S., and Parkinson, G. N. (2003) The structure of telomeric DNA. *Curr. Opin. Struct. Biol. 13*, 275–283.

(3) Eddy, J., and Maizels, N. (2006) Gene function correlates with potential for G4 DNA formation in the human genome. *Nucleic Acids Res. 34*, 3887–3896.

(4) Siddiqui-Jain, A., Grand, C. L., Bearss, D. J., and Hurley, L. H. (2002) Direct evidence for a G-quadruplex in a promoter region and its targeting with a small molecule to repress c-MYC transcription. *Proc. Natl. Acad. Sci. U.S.A. 99*, 11593–11598.

(5) Simonsson, T., Pecinka, P., and Kubista, M. (1998) DNA tetraplex formation in the control region of c-myc. *Nucleic Acids Res. 26*, 1167–1172.

(6) Rankin, S., Reszka, A. P., Huppert, J., Zloh, M., Parkinson, G. N., Todd, A. K., Ladame, S., Balasubramanian, S., and Neidle, S. (2005) Putative DNA Quadruplex Formation within the Human c-kit Oncogene. *J. Am. Chem. Soc. 127*, 10584–10589.

(7) Cogoi, S., and Xodo, L. E. (2006) G-Quadruplex formation within the promoter of the KRAS proto-oncogene and its effect on transcription. *Nucleic Acids Res. 34*, 2536–2549.

(8) Dai, J., Dexheimer, T. S., Chen, D., Carver, M., Ambrus, A., Jones, R. A., and Yang, D. (2006) An Intramolecular G-Quadruplex Structure with Mixed Parallel/Antiparallel G-Strands Formed in the Human BCL-2 Promoter Region in Solution. *J. Am. Chem. Soc. 128*, 1096–1098.

(9) Sun, D., Liu, W. J., Guo, K., Rusche, J. J., Ebbinghaus, S., Gokhale, V., and Hurley, L. H. (2008) The proximal promoter region of the human vascular endothelial growth factor gene has a G-quadruplex structure that can be targeted by G-quadruplex-interactive agents. *Mol. Cancer Ther. 7*, 880–889.

(10) De Armond, R., Wood, S., Sun, D., Hurley, L. H., and Ebbinghaus, S. W. (2005) Evidence for the Presence of a Guanine Quadruplex Forming Region within a Polypurine Tract of the Hypoxia Inducible Factor 1α Promoter. *Biochemistry 44*, 16341–16350.

(11) Hurley, L. H. (2002) DNA and its associated processes as targets for cancer therapy. *Nat. Rev. Cancer 2*, 188–200.

(12) Nelson, S. M., Ferguson, L. R., and Denny, W. A. (2004) DNA and the chromosome: Varied targets for chemotherapy. *Cell Chromosome 3*, 2.

(13) Hurley, L. H. (2001) Secondary DNA structures as molecular targets for cancer therapeutics. *Biochem. Soc. Trans. 29*, 692–696.

(14) Arora, A., Balasubramanian, C., Kumar, N., Agrawal, S., Ojha, R. P., and Maiti, S. (2008) Binding of berberine to human telomeric quadruplex: Spectroscopic, calorimetric and molecular modeling studies. *FEBS J. 275*, 3971–3983.

(15) Cocco, M. J., Hanakahi, L. A., Huber, M. D., and Maizels, N. (2003) Specific interactions of distamycin with G-quadruplex DNA. *Nucleic Acids Res. 31*, 2944–2951.

(16) Sun, H., Xiang, J., Tang, Y., Xu, G., Zhang, Y., Zhang, H., and Xu, L. (2006) Spectroscopic studies of the interaction between quercetin and G-quadruplex DNA. *Bioorg. Med. Chem. Lett. 16*, 3586–3589.

(17) Ho, C. Y., Wong, C. H., and Li, H. Y. (2008) Perturbation of the chromosomal binding of RCC1, Mad2 and survivin causes spindle assembly defects and mitotic catastrophe. *J. Cell. Biochem. 105*, 835–846.

(18) Chen, F. M., Sha, F., Chin, K. H., and Chou, S. H. (2003) Binding of Actinomycin D to Single-Stranded DNA of Sequence Motifs d (TGTCTnG) and d(TGTnGTCT). *Biophys. J. 84*, 432–439.

(19) Yoo, H., and Rill, R. L. (2001) Actinomycin D Binding to Unstructured, Single-stranded DNA. *J. Mol. Recognit. 14*, 145–150.

(20) Wadkins, R. M., Jares-Erijman, E. A., Klement, R., Rudiger, A., and Jovin, T. M. (1996) Actinomycin D Binding to Single-stranded DNA: Sequence Specificity and Hemi-intercalation Model from Fluorescence and ^{1}H NMR Spectroscopy. *J. Mol. Biol. 262*, 53–68.

(21) Chen, F. M., and Sha, F. (2001) Actinomycin D Binds Strongly to d(TGTCATTG), a Single-Stranded DNA Devoid of GpC Sites. *Biochemistry 40*, 5218–5225.

(22) Bailey, S. A., Graves, D. E., and Rill, R. (1994) Binding of Actinomycin D to the T(G)nT Motif of Double-Stranded DNA: Determination of the Guanine Requirement in Nonclassical, Non-GpC Binding Sites. *Biochemistry 33*, 11493–11500.

(23) Jeeninga, R. E., Huthoff, H. T., Gultyaev, A. P., and Berkhout, B. (1998) The mechanism of actinomycin D-mediated inhibition of HIV-1 reverse transcription. *Nucleic Acids Res. 26*, 5472–5479.

(24) Wadkins, R. M., Vladu, B., and Tung, C. S. (1998) Actinomycin D Binds to Metastable Hairpins in Single-Stranded DNA. *Biochemistry 37*, 11915–11923.

(25) Wadkins, R. M., Tung, C. S., Vallone, P. M., and Benight, A. S. (2000) The Role of the Loop in Binding of an Actinomycin D Analog to Hairpins Formed by Single-Stranded DNA. *Arch. Biochem. Biophys. 384*, 199–203.

(26) Nagesh, N., and Chatterji, D. (1995) Ammonium ion at low concentration stabilizes the G-quadruplex formation by telomeric sequence. *J. Biochem. Biophys. Methods 30*, 1–8.

(27) Paramasivan, S., and Bolton, P. H. (2008) Mix and measure fluorescence screening for selective quadruplex binders. *Nucleic Acids Res. 36*, e106.

(28) Hudson, J. S., Brooks, S. C., and Graves, D. E. (2009) Interactions of Actinomycin D with Human Telomeric G-Quadruplex DNA. *Biochemistry 48*, 4440–4447.

(29) Lutz, W., Leon, J., and Eilers, M. (2002) Contributions of Myc to tumorigenesis. *Biochim. Biophys. Acta 1602*, 61–71.

(30) Vita, M., and Henriksson, M. (2006) The Myc oncoprotein as a therapeutic target for human cancer. *Semin. Cancer Biol. 16*, 318–330.

(31) Wiman, K. G., Clarkson, B., Hayday, A. C., Saito, H., Tonegawa, S., and Hayward, W. S. (1984) Activation of a translocated c-myc gene: Role of structural alterations in the upstream region. *Proc. Natl. Acad. Sci. U.S.A. 81*, 6798–6802.

(32) Berberich, S. J., and Postel, E. H. (1995) PuF/NM23-H2/NDPK-B transactivates a human c-myc promoter-CAT gene via a functional nuclease hypersensitive element. *Oncogene 10*, 2343–2347.

(33) Vaquero, A., and Portugal, J. (1998) Modulation of DNA-protein interactions in the P1 and P2 c-myc promoters by two intercalating drugs. *Eur. J. Biochem. 251*, 435–442.

(34) Lemarteleur, T., Gomez, D., Paterski, R., Mandine, E., Mailliet, P., and Riou, J. F. (2004) Stabilization of the c-myc gene promoter quadruplex by specific ligands' inhibitors of telomerase. *Biochem. Biophys. Res. Commun. 323*, 802–808.

(35) Freyer, M. W., Buscaglia, R., Kaplan, K., Cashman, D., Hurley, L. H., and Lewis, E. A. (2007) Biophysical Studies of the c-MYC NHE III1 Promoter: Model Quadruplex Interactions with a Cationic Porphyrin. *Biophys. J. 92*, 2007–2015.

(36) Jennewein, S., and Waring, M. J. (1997) Footprinting of echinomycin and actinomycin D on DNA molecules asymmetrically substituted with inosine and/or 2,6-diaminopurine. *Nucleic Acids Res. 25*, 1502–1510.

(37) Kumar, N., and Maiti, S. (2008) A thermodynamic overview of naturally occurring intramolecular DNA quadruplexes. *Nucleic Acids Res. 36*, 5610–5622.
(38) Jenkins, T. C. (1997) Optical Absorbance and Fluorescence Techniques for Measuring DNA-Drug Interactions. In Drug-DNA interaction protocols (Methods in molecular biology) (Fox, K. R., Ed.) pp 195−218, Springer-Verlag, New York.
(39) Wang, J., Wang, H., Li, Z., Wu, Q., Lathia, J. D., McLendon, R. E., Hjelmeland, A. B., and Rich, J. N. (2008) c-Myc Is Required for Maintenance of Glioma Cancer Stem Cells. *PLoS ONE 3*, e3769.
(40) Hall, C. L., Bafico, A., Dai, J., Aaronson, S. A., and Keller, E. T. (2005) Prostate Cancer Cells Promote Osteoblastic Bone Metastases through Wnts. *Cancer Res. 65*, 7554–7560.
(41) Ambrus, A., Chen, D., Dai, J., Jones, R. A., and Yang, D. (2005) Solution Structure of the Biologically Relevant G-Quadruplex Element in the Human c-MYC Promoter. Implications for G-Quadruplex Stabilization. *Biochemistry 44*, 2048–2058.
(42) Kalousek, I., Brodska, B., Otevrelova, P., and Röselova, P. (2007) Actinomycin D upregulates proapoptotic protein Puma and downregulates Bcl-2 mRNA in normal peripheral blood lymphocytes. *Anticancer Drugs 18*, 763–772.
(43) Tan, J. H., Lu, Y. J., Huang, Z. S., Gu, L. Q., and Wu, J. Y. (2007) Spectroscopic studies of DNA binding modes of cation-substituted anthrapyrazoles derived from emodin. *Eur. J. Med. Chem. 42*, 1169–1175.
(44) Paramasivan, S., Rujan, I., and Bolton, P. H. (2007) Circular dichroism of quadruplex DNAs: Applications to structure, cation effects and ligand binding. *Methods 43*, 324–331.
(45) Seenisamy, J., Rezler, E. M., Powell, T. J., Tye, D., Gokhale, V., Joshi, C. S., Siddiqui-Jain, A., and Hurley, L. H. (2004) The Dynamic Character of the G-Quadruplex Element in the c-MYC Promoter and Modification by TMPyP4. *J. Am. Chem. Soc. 126*, 8702–8709.
(46) Bugaut, A., and Balasubramanian, S. (2008) A sequence-independent study of the influence of short loop lengths on the stability and topology of intramolecular DNA G-quadruplexes. *Biochemistry 47*, 689–697.
(47) Waller, Z. A., Shirude, P. S., Rodriguez, R., and Balasubramanian, S. (2008) Triarylpyridines: A versatile small molecule scaffold for G-quadruplex recognition. *Chem. Commun. 28*, 1467–1469.
(48) Kumar, N., Basundra, R., and Maiti, S. (2009) Elevated polyamines induce c-MYC overexpression by perturbing quadruplex-WC duplex equilibrium. *Nucleic Acids Res.*, No. gkp196.
(49) Seenisamy, J., Bashyam, S., Gokhale, V., Vankayalapati, H., Sun, D., Siddiqui-Jain, A., Streiner, N., Shin-Ya, K., White, E., Wilson, W. D., and Hurley, L. H. (2005) Design and synthesis of an expanded porphyrin that has selectivity for the c-MYC G-quadruplex structure. *J. Am. Chem. Soc. 127*, 2944–2959.
(50) Rosenwald, I. B., Setkov, N. A., Kazakov, V. N., Chen, J. J., Ryazanov, A. G., London, I. M., and Epifanova, O. I. (1995) Transient inhibition of protein synthesis induces expression of proto-oncogenes and stimulates resting cells to enter the cell cycle. *Cell Proliferation 28*, 631–644.
(51) Shiramizu, B., and Magrath, I. (1990) Localization of breakpoints by polymerase chain reactions in Burkitt's lymphoma with 8;14 translocations. *Blood 75*, 1848–1852.